Acta Materialia 230 (2022) 117841

Contents lists available at ScienceDirect

Acta Materialia

journal homepage: www.elsevier.com/locate/actamat

Full length article

Size scaling in bi-crystalline Cu micropillars containing a coherent twin boundary

Reza Hosseinabadi[a], Heinz Riesch-Oppermann[b], James P. Best[a], Gerhard Dehm[a,*], Christoph Kirchlechner[a,b]

[a] Max-Planck-Institut für Eisenforschung GmbH, Germany
[b] Institute for Applied Materials, Karlsruhe Institute of Technology, Germany

ARTICLE INFO

Article history:
Received 30 November 2021
Revised 24 February 2022
Accepted 11 March 2022
Available online 12 March 2022

Keywords:
Dislocation
Twin boundary
Slip transmission
Micro pillars
Compression

ABSTRACT

The impact of a coherent twin boundary (CTB) on the size scaling of the shear stress in micropillar compression tests has been investigated through microcompression of bi-crystalline pillars containing a vertical CTB, as well as single-crystalline pillars in three different nominal diameters of 1, 3 and 5 µm. While both, single- and bi-crystalline pillar results follow the size scaling trend typically observed in micropillars, namely "smaller is stronger", we could identify a size-dependent contribution of the CTB in the increase of the shear stress at 2% strain ($\tau_{2\%}$). A probabilistic analysis was performed to quantify the magnitude of the effect and to separate the CTB contribution from the single crystal size scaling contribution of the strength increase. The CTB-related strengthening was most prominent for smaller pillars and tended to be small for larger pillar diameters. The behavior can be explained by attributing an excess dislocation curvature in the scaling law according to the double-hump dislocation line shape model for bi-crystals, which requires parallel alignment of the dislocation line and the Burgers vector at the CTB.

1. Introduction

Grain boundaries (GBs) mediate the mechanical behavior of polycrystalline metals. Employing the idea that GBs serve as obstacles to dislocation motion, the classic Hall-Petch relationship explained empirically that the strength is proportional to the inverse square root of the grain size [1,2]. Nonetheless, more recent studies show that GBs do not always act as a barrier to dislocation motion. Dislocations can be nucleated [3–5], absorbed [3,6], reflected [7,8], or even transmitted through GBs [7,9,10]. In metals with grain sizes smaller than 100 nm, GBs can also substantially contribute to plastic deformation by means of GB sliding [11], grain rotation [12], and shear-coupled GB motion [13].

Σ3{111} coherent twin boundaries are ubiquitous in face centered cubic (FCC) metals [14]. Arising from the interaction of lattice dislocations with GBs during deformation, twin boundaries can endow exceptional properties to polycrystalline materials such as concurrent high strength and ductility [15]. Thus, understanding the precise mechanisms of twin boundary-dislocation interaction is pivotal for improving the mechanical behavior of metals. These mechanisms include dislocation transmission [3], detwinning [16], dislocation emission [5], and/or absorption of dislocations at twin boundaries [17].

Slip transmission of {111} < 110 > dislocations through Σ3{111} coherent twin boundaries (CTB) in FCC crystals can occur via two modes, depending on the crystallographic direction of the involved grains. In the "hard" mode, the Burgers vector of the lattice dislocation cannot be conserved in transmission. This leads to complex transmission states and results in higher transmission stresses leading to dislocation pile-ups [17,18]. In the "soft" or "ideal" mode, the Shockley partials of lattice dislocations constrict to form a perfect screw dislocation which is shared by both grains adjacent to the twin boundary. The possibility to conserve the Burgers vector of a screw dislocation in both grains facilitates a cross-slip-like transmission to the other grain [17].

Ideal slip transmission can be explained similarly to Friedel-Escaig-like cross-slip [10], and has been the focus of much experimental [3,10,19–24] and computational [17,25,26] research. Quantifying the stress required for slip transmission can shed light on the underlying mechanism of dislocation-CTB interaction. In contrast to a transmission stress of 510 MPa in copper calculated by molecular dynamics simulations by Jin et al. [17], Caillard et al. measured the shear stress required for constricting partial dislocations for cross-slip to be much lower, 24 ± 2 MPa, using a technique to produce bursts of cross slip at the yield point [27]. Con-

* Corresponding author.
E-mail address: dehm@mpie.de (G. Dehm).

https://doi.org/10.1016/j.actamat.2022.117841

sidering the low stress values for cross-slip, it is understandable that *in situ* transmission electron microscopy (TEM) compression of bi-crystalline pillars showed no pile-up of dislocations at the CTB at stresses as high as 500 MPa [21]. Due to the sub-micron dimensions of TEM samples, high stresses for the activation of dislocation sources are required, which is more than sufficient for transmission to occur.

Using *in situ* μLaue diffraction to investigate the micrometer-sized samples containing a CTB, Malyar et al. also observed no pile-up at the CTB and stated that the ideal transmission occurs at shear stresses as low as 17 MPa [22]. Malyar et al. tested single- and bi-crystalline pillars (Sxx and Bxx, respectively) with a diameter of 3 μm to measure the shear stress difference due to the presence of the CTB [10]. The micropillars deform at shear stresses higher than what is required for ideal cross-slip-like slip transmission, so a similar stress for single and bi-crystalline samples (Sxx, Bxx) could be expected (similar to the observations of Liebig et al. in bi-crystalline micropillars for <112> oriented samples [23]). However, increasing the number of tested samples to more than 120 facilitated a statistical analysis that resulted in a shear stress difference ($\Delta\tau_{2\%}$) of 5-7 MPa between Sxx and Bxx pillars at a nominal sample diameter of 3 μm [10]. The small $\Delta\tau_{2\%}$ indicates that the dislocation source size is not truncated by the CTB and expands from one grain to another. This is in contrast to pillars containing a large angle grain boundary [28], where the pillar strength is increased with regards to $d/2$ due to the size effect [29]. Malyar et al. proposed a double-hump shape of the dislocation line to explain the unexpectedly low $\Delta\tau_{2\%}$ [10]. In this model, the dislocation experiences an additional curvature (penalty curvature) near the CTB in Bxx pillars due to the parallel alignment of the dislocation line to the CTB plane, required to form a pure screw character to cross slip (Fig. 1b and Fig. 1d).

Direct observation of dislocation transmission at low stresses via the double-hump was so far impossible, and as such, no experimental verification exists to support the assumption of dislocation curvature effects in micropillars. However, if the additional curvature is responsible for the strength increase of Bxx pillars, it can be expected that $\Delta\tau_{2\%}$ increases with decreasing pillar sizes, as the additional curvature compared to the whole dislocation curvature is relatively larger. Therefore, a larger strengthening effect due to the CTB (a larger $\Delta\tau_{2\%}$) is expected in smaller diameters. The effect of the pillar geometry on different dislocation line shape in Sxx and Bxx pillars based on the double-hump model is shown schematically in Fig. 1.

The expected size-dependence of $\Delta\tau_{2\%}$ can be understood using the analogy of dislocation curvature controlled dislocation sources, in the simplest case to a Frank-Read source. In a Frank-Read source the critical shear stress τ required for the spontaneous source operation is inversely related to the distance of the pinning points ($2L$ in Fig. 1a and $2(L_1-\tilde{L})$ in Fig. 1b) following Eq. (1) using the shear modulus G and the Burgers vector b,

$$\tau_{Sxx} \propto \frac{Gb}{2L} \tag{1a}$$

$$\tau_{Bxx} \propto \frac{Gb}{2\left(L-\tilde{L}\right)} \tag{1b}$$

In the pillar source-size dominated regime one can assume that the dislocation source size scales with the pillar diameter (d), which can be used to rewrite Eq. (1),

$$\tau_{Sxx} \propto \frac{Gb}{d} \tag{2a}$$

$$\tau_{Bxx} \propto \frac{Gb}{d-\tilde{d}} \tag{2b}$$

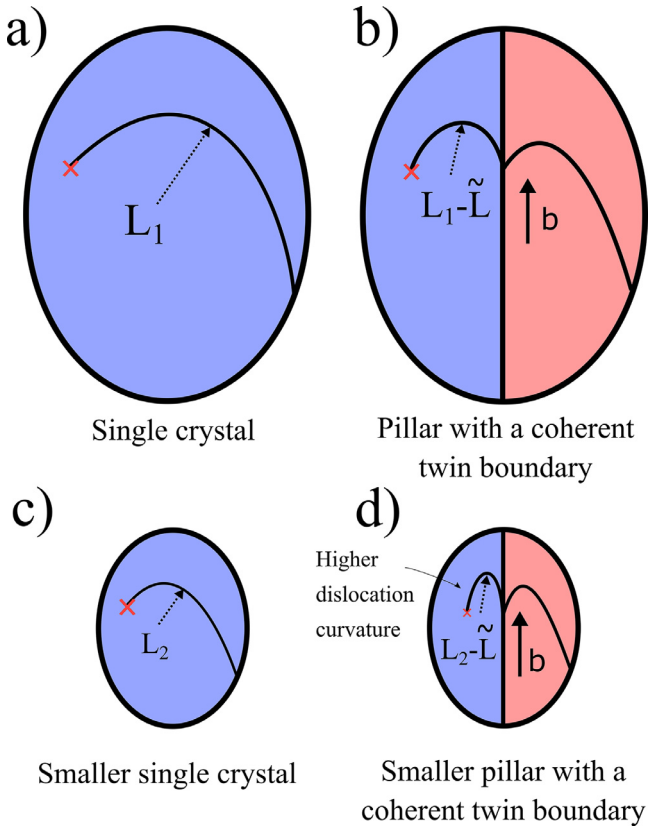

Fig. 1. Schematic showing the operation of a dislocation source in the slip plane in a a) large single crystal; b) a large bi-crystalline pillar containing a CTB; c) a small single crystal; d) a small bi-crystalline pillar containing a CTB. In the case of pillars with a CTB, dislocation constriction near the CTB is required so that the dislocation line aligns parallel to the Burgers vector, so it can cross-slip to the next grain. This causes a double-hump shape of the dislocation line that results in an extra curvature compared to Sxx pillars. The extra or penalty curvature can be interpreted by the decrease in the effective dislocation source size like $L_1-\tilde{L}$ in (b). In smaller bi-crystalline pillars (d), the ratio of the penalty curvature to the existing curvature line is larger; therefore, a higher $\Delta\tau_{2\%}$ is expected.

Notably, Eq. (2) uses the pillar diameter d as the characteristic length scale instead of the actual dislocation source size $2L$ (which is not accessible in micron-sized pillars). The shear stress difference of Sxx and Bxx ($\Delta\tau$) can then be written as:

$$\Delta\tau = \tau_{Bxx} - \tau_{Sxx} = \frac{Gb}{d-\tilde{d}} - \frac{Gb}{d} = \frac{Gb\tilde{d}}{d\left(d-\tilde{d}\right)} \tag{3}$$

The term $d-\tilde{d}$ (and not $\tilde{d}$) is the characteristic length scale of the Bxx pillars, which is smaller than d in Sxx pillars. No direct measurement of $\tilde{d}$ (or better to say $d-\tilde{d}$) is currently possible, as during compression, the bowing of the dislocation takes place within the microscale pillar volume. Based on Eq. (3) and assuming a constant $\tilde{d}$ (as a first order approximation), one expects a negligible $\Delta\tau$ for large pillar diameters, where $\tilde{d}/(d-\tilde{d})$ is relatively small. In contrast, a larger $\Delta\tau$ is expected for pillars with small diameter.

Since a direct observation of the double hump in micron sized samples remains impossible, we aimed to measure the size-scaling behavior of the shear stress difference at 2% strain ($\Delta\tau_{2\%}$) of Sxx and Bxx pillars. As micron-sized compression tests of metals shows stochastic behavior due to the distribution of dislocation sources, multiple measurements for each size were required. For this purpose, 63 copper Sxx and 19 Bxx (containing CTB) micropillars were fabricated and compressed at three different nominal diameters of 1, 3, and 5 μm. To obtain the $\Delta\tau_{2\%}$, a statistical analysis was

performed to decouple the additional strengthening effect of the CTB in Bxx from the size-effect seen for both, Sxx and Bxx. Subsequently, the experimental findings were compared to the physical model derived from the double-hump shape to get a quantitative insight into the role of geometrical constraints on the dislocation shape during ideal slip transmission through CTB.

2. Experimental details and data analysis

2.1. Sample fabrication

The Bridgman technique was employed to fabricate a bulk bi-crystalline sample containing a vertical Σ3{111} CTB from 99.88 at.% pure copper. Electro-discharge machining was used to cut 0.5 mm thin slices of the bi-crystalline sample with a nominal surface normal of $<123>$also corresponding to the compression direction. Slices were next ground, polished, and electrochemically etched using phosphoric acid at 15 V for 45 s to achieve a flat surface without GB grooving as described in Ref. [30]. Cylindrical micropillars were milled using a focused ion beam (FIB, Zeiss Auriga®) workstation in three steps with milling currents ranging from 16 nA to 240 pA. The micropillars were fabricated at nominal diameter sizes of 1, 3, and 5 µm, with an aspect ratio of 2-3 to suppress buckling instabilities. The pillars were milled within one of the two single crystalline regions (Sxx) or at the coherent twin boundary (Bxx). There were in total 96 pillars produced, out of which 82 were tested successfully (63 Sxx and 19 Bxx micropillars milled at the twin boundary).

2.2. Mechanical testing

Compression of 3 µm and 5 µm pillars was performed using an ASMEC UNAT 2, while due to increased load resolution a Bruker Hysitron PI 88 was employed to compress the 1 µm pillars. All tests were performed in displacement controlled mode at a strain rate of 10^{-3} s^{-1}. To reduce the effect of lateral constraints, each pillar was unloaded at about every 5% of strain to reduce the instrumental constraints [22,31,32]. All tests were conducted *in situ* inside the Zeiss Gemini 500® scanning electron microscopy (SEM), and were followed by *post mortem* imaging using secondary electrons in an in-lens detector with the acceleration voltage of 5 kV to verify the slip traces on the surface. The *post mortem* images were used to validate that slip occurred on one single slip system at each grain, which has the highest Schmid factor.

2.3. Analysis of compression data

The pillar diameter was measured at both top and bottom cross-section. An average of the top and bottom diameters of each pillar was used to determine the engineering stress. A Mathematica® script was utilized to calculate the stress-strain data from the force-displacement input. The stress at an engineering strain of 2% was chosen for analysis to minimize the impact of dislocation-dislocation interactions, which becomes more prominent at higher strains. The highest Schmid factor for each grain was calculated and used to obtain the shear stress at 2% engineering strain, denoted as $\tau_{2\%}$. This was done to remove the impact of the slight deviation from the nominal compression direction. In the case of Bxx pillars, the average value of the Schmid factor of the two grains was utilized for shear stress calculation. The error bars of the stress, resulting from uncertainties in force and displacement measurements were calculated for each data point. This is explained in detail in the supplementary file (see S1).

To fit the stress data over the whole pillar diameter range, a continuous analysis was conducted. Applying the approach of Dou and Derby [33], a power-law formulation was used to describe micropillar size effects:

$$\tau_{2\%} = \tau_0 + \frac{k}{d^n} \tag{4}$$

where τ_0 is the bulk yield shear stress, k is the strengthening coefficient, and n is the size scaling exponent. A weighted non-linear least squares (NLLSQ) analysis was used to determine the parameters of the power-law relation. Uncertainties resulting from force and diameter recordings for the stress measurements of each experiment were taken into the account through a weighted sum-of-squares criterion. The uncertainties of the power-law fit were calculated in terms of confidence bands around each fit. To separate the size-effect from the strengthening caused by the presence of CTB, a joint model was developed to take the two effects on the different diameters into account.

3. Results

Single crystalline micropillars (Sxx) or micropillars containing a CTB (Bxx) parallel to the loading direction were compressed to a final strain of ca. 5 - 15% and then imaged using SEM. *Post mortem* imaging for the Sxx pillars of different sizes (not shown) showed the expected parallel slip traces, indicating that only the primary slip system was activated. In the case of Bxx pillars shown in Fig. 2, the glide traces of the two grains meet at the CTB and form a dove-tail shaped slip pattern at the pillar surface, irrespective of the pillar size. This is well known and agrees with the observations of other studies on bi-crystalline micropillar specimens [10,22,23,28,34].

The shear stress at a strain of 2% ($\tau_{2\%}$) was then determined for each pillar from load-displacement data based on the micropillar geometries determined by SEM imaging. The stress-strain curves of the 3 representative Bxx pillars with different diameters are shown in Fig. 2d. The curves exhibit size-scaling and load drops typical for small scale mechanical testing. The single data points of both Sxx and Bxx with their individual error bars, as well as the best power-law fit for Sxx and Bxx and their 68% confidence belts are shown in Fig. 3. For the nominal pillar sizes of 3 and 5 µm, the standard error bars from measurement are smaller than the plotting symbols. As shown in Fig. 3, for all performed tests, the diagram $\tau_{2\%}$ versus diameter highlights a clear size effect of "smaller is stronger", along with a more stochastic response in the flow stress for smaller micropillars with approximately 1 µm diameter. Comparing the two curves against pillar diameter, it is evident that a significant non-zero $\Delta\tau_{2\%}$ is present at smaller diameters, while the fitted curves and their confidence belts overlap at larger pillar diameters.

The data presented in Fig. 3 was then fitted with the power-law model based on Eq. (4) for the shear stress of Sxx and Bxx ($\tau_{Sxx,2\%}$, $\tau_{Bxx,2\%}$, respectively). The resulted parameters are shown in Table 1. Table 1 additionally gives the 95% confidence limits of the best fit parameters that are obtained from the non-linear least squares analysis.

While the best fit parameter estimates and their estimated uncertainties provide some information on the overall quality of the NLLSQ approximation, we would rather have some information about the uncertainty in the fitting curve itself. For this purpose, we calculate the probability that a future measurement will lie within a certain distance above or below our predictive curve. This probability depends on the global approximation error of our fit (in terms of the mean sum of squares, MSS) and on the covariance matrix of the estimated model parameters as well as on the local derivative of the model function with respect to the parameters. The calculations are provided in the supplementary file (see S2). This probability can be visualized in terms of e.g. 68% prediction

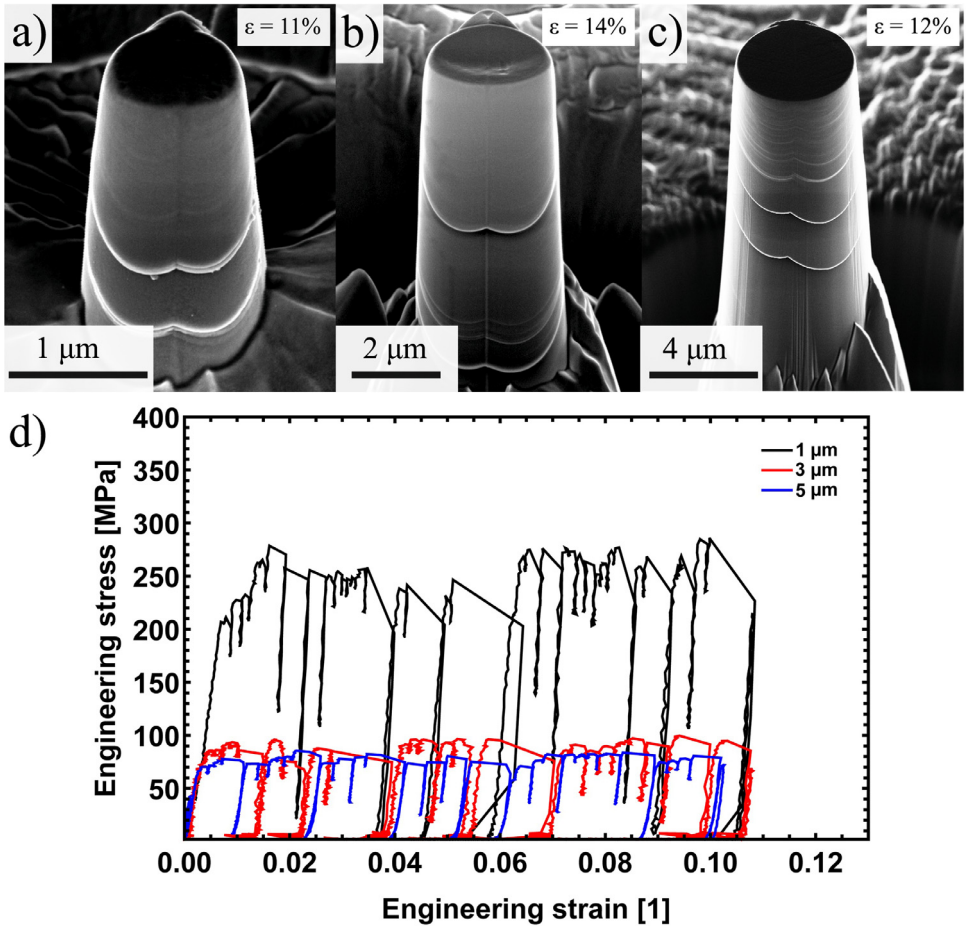

Fig. 2. Post mortem SEM micrographs of Bxx pillars with nominal diameter of 1 μm (a), 3 μm (b), and 5 μm (c) compressed at a strain rate of 10^{-3} s^{-1}. Nominal compression direction is < 123 > . (d) shows the strain-stress curves of three representative Bxx pillars that are 1, 3 and 5 μm in diameter.

Table 1
Optimized fit parameters for Sxx and Bxx pillars from the NLLSQ analysis based on Eq. (4). The optimized parameters for the joint analysis (see Eq. (6)) are also shown in the table.

	Number of samples	τ_0 (MPa)	$\boldsymbol{k}$	$\boldsymbol{n}$ (1)	$\tilde{\boldsymbol{d}}$ (μm)
$\tau_{Sxx,2\%}$	63	23.6 ± 7.2	82.7 ± 6.7	1.10 ± 0.30	-
$\tau_{Bxx,2\%}$	19	28.7 ± 6.7	112.3 ± 12.5	1.38 ± 0.33	-
$\tau_{joint,2\%}$	82	23.8 ± 5.8	82.0 ± 6.1	1.10 ± 0.24	0.27 ± 0.08

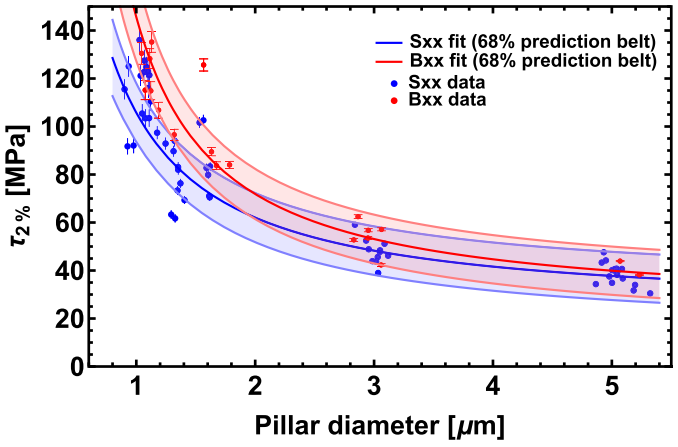

Fig. 3. The shear stress at 2% strain vs. pillar diameter for Bxx and Sxx pillars with their individual error bars. The best fit model of each pillar type and the 68% confidence belt (corresponding to the standard error of the fit) are also shown.

bands around the model prediction curve as a function of the pillar diameter d. Fig. 4. shows the probability density function (PDF) curves $Prob[\tau_{Sxx}]$ as well as $Prob[\tau_{Bxx}]$ from which these bounds are obtained for two diameter values, $d = 1$ μm and $d = 5$ μm. While the two PDF curves for 5 μm are nearly identical (see also the overlap of the 68% confidence belts in Fig. 3 at $d = 5$ μm), a pronounced shift towards higher strength is observed for the PDF curves at $d = 1$ μm (corresponding to the separation of the prediction belts in Fig. 3 at d around 1 μm).

While the prediction bands give some qualitative insight into the strength behavior of single- and bi-crystalline pillars in the observed diameter range, a quantitative analysis is preferable in order to assess the strength of the CTB effect for a given pillar diameter. In other words, we want to know how plausible it is that the Bxx PDF shown in Fig. 4 for $\tau_{2\%}$ at two diameters is located towards larger values compared to the Sxx PDF. We aim to obtain this information in the whole range of pillar diameters.

This can be done with the help of the predictive probability curves that are obtained from the predictive probability distributions $Prob[\tau_{Sxx}]$, $Prob[\tau_{Bxx}]$ as function of the diameter d. Since the

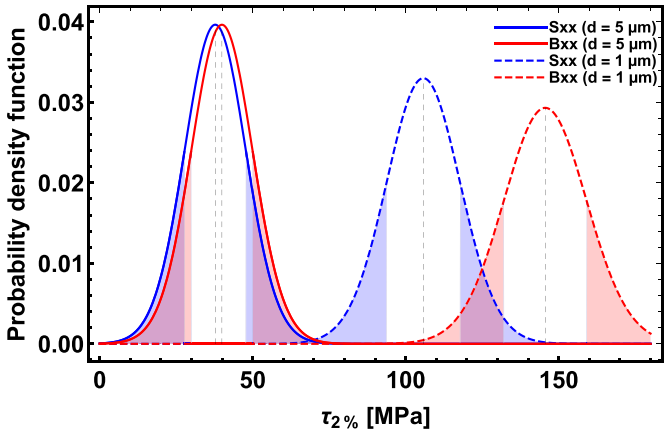

Fig. 4. Probability density function of the predictive distribution around the fit curve, corresponding to Sxx (blue) and Bxx (red) at 1 and 5 μm. The peak of each curve (corresponding to the fit curve) is marked by vertical dashed lines, and the 68% prediction tail areas of each distribution are also shown. Comparing the two sizes of each pillar type indicates that smaller pillars of each type are stronger. However, the shift between Bxx and Sxx shear stress for the two diameters is much larger for the 1 μm pillars.

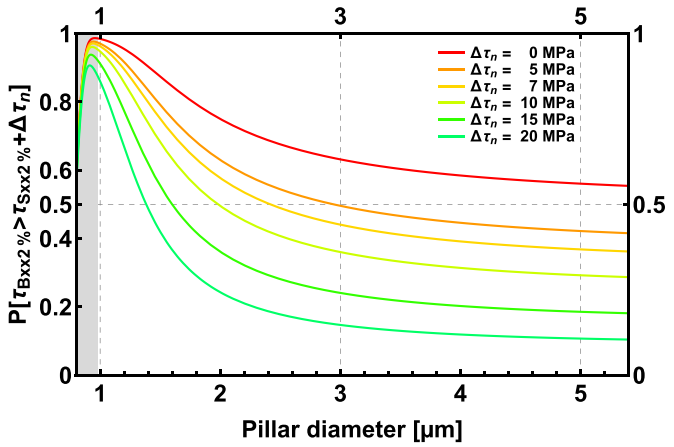

Fig. 5. Probability of τ_{Bxx} being larger than $\tau_{sxx} + \Delta\tau_n$ versus the pillar diameter. The red curve shows this probability for $\Delta\tau_n = 0$, indicating the probability of Bxx pillars being stronger than their Sxx counterparts. The orange curve predicts the probability of τ_{Bxx} being at least 5 MPa stronger than the Sxx pillars, which intersects with 50% probability at 3 μm. The other colors represent the other values for $\Delta\tau_n$. This shows that $\Delta\tau_{2\%}$ increases with decreasing pillar diameter.

pillar data are independently obtained, their joint probability is just the product $Prob[\tau_{Sxx}] * Prob[\tau_{Bxx}]$ of the two individual probabilities. To obtain the probability of a strengthening caused by CTB being larger than a prescribed $\Delta\tau_{2\%}$ (which we call $\Delta\tau_n$), we have to integrate the joint predictive probability over a $[\tau_{Sxx}, \tau_{Bxx}]$ region with $\tau_{Bxx} > \tau_{Sxx} + \Delta\tau_n$:

$$Prob[\tau_{Bxx} > \tau_{Sxx} + \Delta\tau_n] = \int_0^\infty \int_{\tau_{Sxx}+\Delta\tau_n}^\infty Prob[\tau_{Sxx}] * Prob[\tau_{Bxx}] d\ \tau_{Bxx}\ d\ \tau_{Sxx} \quad (5)$$

Setting $\Delta\tau_n = 0$ in Eq. (5), we obtain the probability of having any CTB-caused strengthening at all. Increasing $\Delta\tau_n$ to values larger than zero allows the assessment of positive strengthening effects of CTB. A series of such probability curves with different values for $\Delta\tau_n$ as a function of the pillar diameter is depicted in Fig. 5.

The intersection of the 50% probability gridline with the calculated probability curves provides the desired prediction of $\Delta\tau_{2\%}$. The 50% selection was considered appropriate for two reasons: a) for large diameters it corresponds to $\Delta\tau_n = 0$ (disappearing twin boundary strengthening); b) the 50% level intersects with all $\Delta\tau_n > 0$ curves. The 50% probability meets the dark orange curve (corresponding to $\Delta\tau_n = 5$ MPa) curve at 3 μm and therefore predicts that for diameters below 3μm it is more likely to have a $\Delta\tau_{2\%}$ of at least 5 MPa than less. Notably, Malyar et al. measured the $\Delta\tau_{2\%}$ for 3 μm pillars to be 5-7 MPa [10]. It is worth mentioning that probabilities in diameters less than 1 μm and larger than 5 μm correspond to extrapolation beyond the data range, and due to high uncertainties in diameters less than 1 μm, the model is considered invalid for this regime.

From Fig. 5 it can be concluded that $\Delta\tau_{2\%}$ is not constant in the range of the 1-5 μm pillar diameter. The probability of having a large $\Delta\tau_{2\%}$ is higher at 1 μm and tends towards zero as the pillar diameter increases. This matches our initial assumption based on the double-hump shape of the dislocation line in the Bxx pillars, as the penalty curvature that dislocation needs to pay for ideal slip transmission depends on the characteristic length scale, i.e. pillar diameter.

Next, we aimed to relate the experimental results to the physical understanding of the double-hump shape in the ideal slip transmission Eq. (2). was re-formulated with an indicator variable "Flag" and added to Eq. (4) to describe the shear stress of both Sxx and Bxx in Eq. (6). In this formulation, all data points contribute in the same way to the determination of the parameters; therefore, Eq. (6) is valid for both types of pillars. When Flag = 0, it corresponds to Sxx, while with Flag = 1, the second part of the relation is included, which describes the additional stress caused by the penalty curvature in the Bxx case. This is called the "joint analysis" model and it separates the known size-effect (first term) from the dislocation curvature penalty near the CTB (second term), assuming that they do not interact with each other.

$$\begin{aligned}\tau(d) &= \left(\tau_0 + \frac{k}{d^n}\right)\left(1 + \frac{\tilde{d} * Flag}{d - \tilde{d}}\right) \\ &= \left(\tau_0 + \frac{k}{d^n}\right) \quad \text{(for Sxx pillars)} \\ &= \left(\tau_0 + \frac{k}{d^n}\right)\left(1 + \frac{\tilde{d}}{d - \tilde{d}}\right) \quad \text{(for Bxx pillars)}\end{aligned} \quad (6)$$

Eq. (6) was then fit to the micropillar data using the shear stress at 2% strain, pillar diameter, and Flag value (Fig. 6). Joint analysis parameters obtained from fitting all datasets are reported in Table 1. The weighted sum of squares of the joint analysis automatically take the number of samples (63 Sxx and 19 Bxx) into account, and gives more weight to the larger data set. The additional consideration of the Bxx data in the joint analysis leads to a reduction in the parameter uncertainties compared to the analysis of the individual data sets, i.e. the (smaller) Bxx data but also to the (larger) Sxx data. More importantly, it can clearly be seen that the joint analysis retains the estimators for the parameters τ_0, k and n obtained from the Sxx data, and the Bxx strengthening effect is solely described via the $\tilde{d}$ parameter. It must be noted that all data, regardless of being Sxx or Bxx, can contribute to the joint analysis, meaning that the analysis fit parameters (τ_0, k, n, and $\tilde{d}$) are valid to describe either pillar type. (For more information regarding the joint analysis, refer to the S3 in the supplementary file)

Notably, n (both in separate and in the joint analysis) is close to one, which indicates that our micropillar compression tests are in a dislocation curvature-controlled regime. Fig. 6 shows both the separate power-law fits for each pillar type and the joint analysis (once for Flag = 1 and once for Flag = 0) with a very good overlay. This indicates that with the added term of the penalty curvature, the joint analysis predicts the Bxx behavior extremely

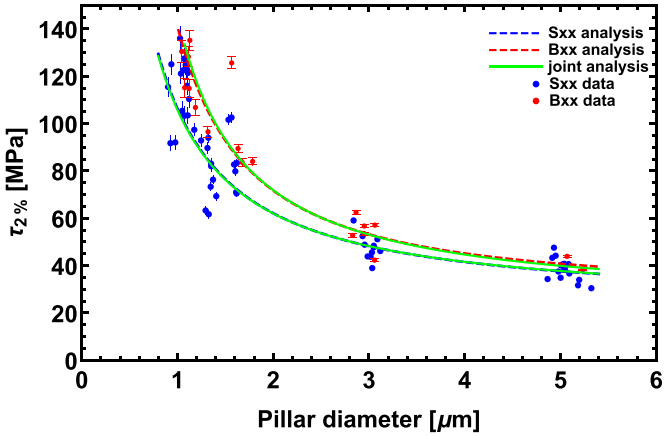

Fig. 6. Shear stress at 2% strain vs pillar diameter of both Bxx and Sxx pillars. The best power-law fits for the Sxx data set (blue curve) and Bxx (red curve) is also shown. The green curves correspond to the joint analysis of the whole data set at Flag=0 for Sxx pillars, and Flag=1 for Bxx pillars. The good match between the individual fits and the two branches of the joint analysis shows that the joint analysis could predict the behavior of the Bxx pillars by adding an additional term to describe the penalty curvature of the dislocation under ideal slip transmission.

closely. Therefore, it can be concluded that the predicated double-hump shape and the dislocation curvature theory can successfully describe the different $\Delta\tau_{2\%}$ values obtained from our experimental data.

An interpretation of the reported value of $\tilde{d}$ in Table 1 can be misleading and caution should be applied, as it is only intended to model the penalty curvature of dislocations in Bxx compared to the Sxx samples. As discussed in the introduction, a direct measurement of the penalty curvature $\tilde{d}$ or the effective source size of Bxx pillars $(d-\tilde{d})$ was not possible in microscale pillars. As a first order approximation $\tilde{d}$ was assumed to be constant. While our joint analysis (Eq. (6)) describes our experimental data with a constant $\tilde{d}$ in the investigated size regime well, this assumption might break down at smaller pillar diameters.

4. Discussion

4.1. Size scaling behavior of bi-crystalline pillars

It is evident from our work, that the general trend of "smaller is stronger" holds true also for CTB containing pillars. Moreover, Bxx pillars are stronger than the Sxx ones across the entire investigated size range. The NLLSQ analysis was employed to obtain the difference of the shear stress at 2% strain between Sxx and Bxx pillars ($\Delta\tau_{2\%}$). The analysis removed the concerns about diameter variations, which affects the pillar strength due to the size-effect. The result of the probabilistic analysis (See Fig. 5) show that $\Delta\tau_{2\%}$ increases with decreasing pillar diameter. At the largest pillar diameter of 5 µm, $\Delta\tau_{2\%}$ reaches values smaller than 5 MPa. Consequently, Sxx and Bxx pillars exhibit differences in their size scaling behavior on the first glance.

The changes of $\Delta\tau_{2\%}$ within the diameter range can be explained using the double-hump shape of the dislocation line in the Bxx pillar, which has been introduced by Malyar et al. [10]. In the presence of a CTB in Bxx pillars, the dislocation needs to fall parallel to the twin boundary. This geometrical constraint requires additional curvature (i.e. additional stress) in order to reorient along with the CTB, so it has a pure screw character and can cross-slip to the next grain (as illustrated in Fig. 1). In smaller diameters, the additional stress compared to the dislocation line tension is relatively large; therefore, a larger strengthening due to CTB (i.e. a larger $\Delta\tau_{2\%}$) is present. This finding is qualitatively in line with the existence of the double-hump shape.

4.2. Decoupling size-effect from CTB-strengthening

While the varying $\Delta\tau_{2\%}$ points towards the double-hump, the penalty curvature of the dislocation line could be better examined by comparing a model, driven from the double-hump, to the experimental data. In such model, the separation of the strengthening mechanisms (namely size-effect and strengthening caused by CTB) is vital to fundamentally and quantitatively understand the important role of CTBs in the mechanical properties at the micron scale.

It is notable that other models based on possible dislocation-CTB interaction scenarios were also considered. These models include: (i) CTB being no barrier to the transmission, in this case $\Delta\tau_{2\%}$ would be zero; (ii) CTB requiring a fixed stress value to allow the transmission to happen, in other words $\tau_{Bxx}=\tau_{Sxx}+\tau_{transmission}$, in which $\tau_{transmission}$ is a constant value; (iii) CTB being a hard barrier that does not allow the ideal transmission. The small and varying $\Delta\tau_{2\%}$ across the studied diameter range rejects all 3 models; therefore, only the model driven from the double-hump shape was chosen for further analysis. Section S4 of the supplementary file discusses these models based on the calculated probability function.

We assume that in the Sxx pillars, the strength is dictated by the ease of operating a dislocation source. According the double-hump mechanism, the same should hold for twin boundary pillars, however, the effective source size is smaller due to the dislocation curvature near CTB. Given that the two strengthening mechanisms are independent, i.e. there is no mutual interaction, this separation can be done in the joint analysis based on Eq. (6).

Remarkably, the joint analysis can successfully describe both the Sxx and Bxx data. The observation is remarkable because both, the dislocation source size effect as well as the double-hump are dominated by dislocation curvatures, and an influence of one effect on the other seems to be reasonable. Nevertheless, the joint analysis describes the data well and one can conclude, that the mutual interaction of the two mechanisms can be neglected in the investigated size regime.

4.3. Extrapolation towards smaller and larger dimensions

$\Delta\tau_{2\%}$ was investigated in the pillar diameter range from 1 to 5 µm. While describing our data within this size regime worked well (see Section 4.2), an extrapolation of the twin boundary behavior to larger and smaller twin spacing remains challenging. At the upper size limit, at 5µm, $\Delta\tau_{2\%}$ is as low as 5 MPa. We postulate, that further increasing the pillar diameter results in an ever smaller $\Delta\tau_{2\%}$, as long as the shear stress on the transmitting slip system exceeds the value for cross slip of pure copper, i.e. 24 ± 2 MPa [27]. The reduction of $\Delta\tau_{2\%}$ is rationalized by any curvature penalty due to the double hump, which vanishes with increasing pillar size (see Eq. (3)). As soon as the minimum shear stress for dislocation cross-slip is not reached anymore, dislocations will not be able to transmit through the boundary and an increased difference of Sxx and Bxx could be prognosticated. However, based on Eq. (4) and the data in Table 1, the aforementioned scenario does not happen for pillars smaller 200 µm. In such large samples however dislocation sources are easily activated and may obscure the effect of a CTB.

The extrapolation to smaller sizes is more challenging; a comparison is best made to nanotwinned materials. Lu et al. reported elevated yield stress of 900 MPa in nanotwinned Cu [35]. Kini et al. recently suggested that the pillar strength scales inversely

with twin spacing. They showed the dislocation curvature in nanotwinned Ag thin films from cross-slip of dislocations across numerous twin boundaries in twin spacing down to 15 nm [24]. Obviously, the dislocation line shape is not a single double-hump in these cases, but rather a periodic bowing out of the dislocations at each grain boundary to facilitate the cross slip. The extrapolation of our data is dangerous because (i) the mechanisms at play might change and (ii) larger scatter of stress data obtained from 1 µm sized pillars render a prediction to smaller diameters challenging:

(i) CTBs frequently contain defects like ledges or Frank partial dislocations, which can act as dislocation sources at high stresses [5]. In the underlying case, we did not see evidence of extensive dislocation source activation at the twin boundary, e.g. by multiple small slip steps. In contrast, in all our cases compatibility of slip with large slip steps is observed. Assuming the model and data in Eq. (1) and Table 1, as well as a dislocation source activation strength in the CTB of 2500 MPa [5], dislocation source activation at the CTB would not happen for pillars larger than ∼50 nm. Such small pillars cannot be tested with high confidence (and low scatter) by micro pillar compression. Besides, as soon as the dislocation splitting width is close to the pillar diameter, partial slip activation is expected and the deformation behavior might be considerably different.

(ii) The scatter in the data is likely not caused by instrumental scatter, rather by the stochastic nature of dislocation slip at the micron scale [36,37]. A significant increase of the sample number is required to understand the strength distribution of even smaller pillars tested here. This, however, is hardly possible because of FIB time required to get sufficient statistics.

4.4. A comment on the probabilistic analysis scheme

A highly detailed probabilistic analysis of the Sxx/Bxx strength could be obtained based on the full analysis over the experimental pillar diameter range, as opposed to a separate analysis of the strength distribution for each nominal pillar diameter. Using the double hump CTB strengthening approach, we obtained predictive probability distributions for the strengths as function of the pillar diameter, from which we could directly calculate (via Eq. (5)) the probability of prescribed CTB strengthening amounts $\Delta\tau_n$, as shown in Fig. 5. Such a direct probability cannot be obtained from the comparison of credibility bands based on a pre-specified credibility level as is common in conventional statistical analysis procedures. We also want to emphasize that this type of analysis can be generalized to multi-twin systems, provided a suitable strengthening model is available or can be hypothesized.

5. Summary and conclusions

Conducting micropillar compression in different nominal diameters showed that Bxx pillars containing a coherent twin boundary (CTB) follow the “smaller is stronger” paradigm, as it has been previously reported for Sxx pillars. The $\Delta\tau_{2\%}$ is larger at smaller diameters, and it tends to values close to a few MPa at 5 µm diameter. A model based on the penalty curvature in double-hump shape was developed to compare with the experimental data. This model in the “joint analysis”, could successfully describe the data. Therefore, we conclude that the geometric constraints (and not the CTB itself) imposed by the transmission slip geometry causes a penalty curvature of the dislocation, which is responsible for the size-dependent strength increase $\Delta\tau_{2\%}$ in CTB containing pillars.

Quantifying the increase of pillar strength, due to the presence of the CTB, $\Delta\tau_{2\%}$, remains challenging, as it requires the separation of the CTB-related contribution from the general size-effect present in both, Sxx as well as Bxx pillars. This separation could successfully be done by our probabilistic analysis, which provided probability curves for the prediction of plausible $\Delta\tau_{2\%}$ amounts over the whole range of the pillar diameters in the experiments. For pillars larger than 5 µm in diameter, the CTB strengthening is expected to be marginal. The extrapolation of the probability curves towards diameters smaller than 1 µm bears large uncertainties to it. The predictive function might be used to determine the strengthening in other CTB-containing systems, for example in nano-twinned structures. Likewise, the probabilistic tools used in the joint analysis can be employed for other similar experimental settings, e.g. in studies that aim at separating the GB strengthening contribution from the general size-effect in case of other GBs.

Declaration of competing interest

The authors declare that they have no known competing financial interests or personal relationships that could have appeared to influence the work reported in this paper.

Acknowledgments

The authors gratefully thank Jürgen Wichert and Dr. Nataliya Limbach-Malyar for producing the Cu bi-crystals and Leon Christiansen for assistance in pillar milling. GD acknowledges the European Research Council for funding part of this project (Grant no. 787446-GB-CORRELATE). Financial support by the Robert Bosch Foundation is gratefully acknowledged by CK.

Supplementary materials

Supplementary material associated with this article can be found, in the online version, at doi:10.1016/j.actamat.2022.117841.

References

[1] E.O. Hall, The deformation and ageing of mild steel: II Characteristics of the Lüders deformation, Proc. Phys. Soc. Sect. B. 64 (1951) 742–747, doi:10.1088/0370-1301/64/9/302.
[2] N.J. Petch, The Cleavage Strength of Polycrystals, J. Iron Steel Inst. 174 (1953) 25–28.
[3] J. Kacher, B.P.P. Eftink, B. Cui, I.M.M. Robertson, Dislocation interactions with grain boundaries, Curr. Opin. Solid State Mater. Sci. 18 (2014) 227–243, doi:10.1016/j.cossms.2014.05.004.
[4] G. Bäro, H. Gleiter, E. Hornbogen, Korngrenzen als Versetzungsquellen, Mater. Sci. Eng. 3 (1968) 92–104, doi:10.1016/0025-5416(68)90023-2.
[5] J. Li, G.M. Pharr, C. Kirchlechner, Quantitative insights into the dislocation source behavior of twin boundaries suggest a new dislocation source mechanism, J. Mater. Res. (2021), doi:10.1557/s43578-021-00253-y.
[6] D.J. Dingley, R.C. Pond, On the interaction of crystal dislocations with grain boundaries, Acta Metall 27 (1979) 667–682, doi:10.1016/0001-6160(79)90018-X.
[7] Z. Shen, R.H. Wagoner, W.A.T. Clark, Dislocation and grain boundary interactions in metals, Acta Metall 36 (1988) 3231–3242, doi:10.1016/0001-6160(88)90058-2.
[8] T.C. Lee, I.M. Robertson, H.K. Birnbaum, An in situ transmission electron microscope deformation study of the slip transfer mechanisms in metals, Metall. Trans. A. 21 (1990) 2437–2447, doi:10.1007/BF02646988.
[9] W.A.T. Clark, R.H. Wagoner, Z.Y. Shen, T.C. Lee, I.M. Robertson, H.K. Birnbaum, On the criteria for slip transmission across interfaces in polycrystals, Scr. Metall. Mater. 26 (1992) 203–206, doi:10.1016/0956-716X(92)90173-C.
[10] N.V. Malyar, B. Grabowski, G. Dehm, C. Kirchlechner, Dislocation slip transmission through a coherent Σ3{111} copper twin boundary: strain rate sensitivity, activation volume and strength distribution function, Acta Mater 161 (2018) 412–419, doi:10.1016/j.actamat.2018.09.045.
[11] H. Van Swygenhoven, P.M. Derlet, Grain-boundary sliding in nanocrystalline fcc metals, Phys. Rev. B - Condens. Matter Mater. Phys. 64 (2001) 1–9, doi:10.1103/PhysRevB.64.224105.
[12] E. Ma, Watching the nanograins roll, Science 305 (2004) 623–624, doi:10.1126/science.1101589.
[13] M. Legros, D.S. Gianola, K.J. Hemker, In situ TEM observations of fast grain-boundary motion in stressed nanocrystalline aluminum films, Acta Mater 56 (2008) 3380–3393, doi:10.1016/j.actamat.2008.03.032.
[14] D.M. Saylor, B.S. El Dasher, A.D. Rollett, G.S. Rohrer, Distribution of grain boundaries in aluminum as a function of five macroscopic parameters, Acta Mater 52 (2004) 3649–3655, doi:10.1016/j.actamat.2004.04.018.

[15] M. Dao, L. Lu, Y.F. Shen, S. Suresh, Strength, strain-rate sensitivity and ductility of copper with nanoscale twins, Acta Mater 54 (2006) 5421–5432, doi:10.1016/j.actamat.2006.06.062.
[16] J. Wang, N. Li, O. Anderoglu, X. Zhang, A. Misra, J.Y. Huang, J.P. Hirth, Detwinning mechanisms for growth twins in face-centered cubic metals, Acta Mater 58 (2010) 2262–2270, doi:10.1016/j.actamat.2009.12.013.
[17] Z.H. Jin, P. Gumbsch, E. Ma, K. Albe, K. Lu, H. Hahn, H. Gleiter, The interaction mechanism of screw dislocations with coherent twin boundaries in different face-centred cubic metals, Scr. Mater. 54 (2006) 1163–1168, doi:10.1016/j.scriptamat.2005.11.072.
[18] Z.H. Jin, P. Gumbsch, K. Albe, E. Ma, K. Lu, H. Gleiter, H. Hahn, Interactions between non-screw lattice dislocations and coherent twin boundaries in face-centered cubic metals, Acta Mater 56 (2008) 1126–1135, doi:10.1016/j.actamat.2007.11.020.
[19] V. Samaee, M. Dupraz, T. Pardoen, H. Van Swygenhoven, D. Schryvers, H. Idrissi, Deciphering the interactions between single arm dislocation sources and coherent twin boundary in nickel bi-crystal, Nat. Commun. 12 (2021) 962, doi:10.1038/s41467-021-21296-z.
[20] P.J. Imrich, C. Kirchlechner, G. Dehm, Influence of inclined twin boundaries on the deformation behavior of Cu micropillars, Mater. Sci. Eng. A. 642 (2015) 65–70, doi:10.1016/j.msea.2015.06.064.
[21] P.J. Imrich, C. Kirchlechner, D. Kiener, G. Dehm, Internal and external stresses: In situ TEM compression of Cu bicrystals containing a twin boundary, Scr. Mater. 100 (2015) 94–97, doi:10.1016/j.scriptamat.2014.12.023.
[22] N.V. Malyar, J.S. Micha, G. Dehm, C. Kirchlechner, Dislocation-twin boundary interaction in small scale Cu bi-crystals loaded in different crystallographic directions, Acta Mater 129 (2017) 91–97, doi:10.1016/j.actamat.2017.02.067.
[23] J.P. Liebig, S. Krauß, M. Göken, B. Merle, Influence of stacking fault energy and dislocation character on slip transfer at coherent twin boundaries studied by micropillar compression, Acta Mater 154 (2018) 261–272, doi:10.1016/j.actamat.2018.05.037.
[24] M.K. Kini, G. Dehm, C. Kirchlechner, Size dependent strength, slip transfer and slip compatibility in nanotwinned silver, Acta Mater 184 (2019) 120–131, doi:10.1016/J.ACTAMAT.2019.11.042.
[25] J.B. Jeon, G. Dehm, Formation of dislocation networks in a coherent Cu Σ3(1 1 1) twin boundary, Scr. Mater. 102 (2015) 71–74, doi:10.1016/j.scriptamat.2015.02.016.
[26] M. Chassagne, M. Legros, D. Rodney, Atomic-scale simulation of screw dislocation/coherent twin boundary interaction in Al, Au, Cu and Ni, Acta Mater 59 (2011) 1456–1463, doi:10.1016/j.actamat.2010.11.007.
[27] D. Caillard, J.L. Martin, Some aspects of cross-slip mechanisms in metals and alloys, J. Phys. 50 (1989) 2455–2473, doi:10.1051/jphys:0198900500180245500.
[28] P.J. Imrich, C. Kirchlechner, C. Motz, G. Dehm, Differences in deformation behavior of bicrystalline Cu micropillars containing a twin boundary or a large-angle grain boundary, Acta Mater 73 (2014) 240–250, doi:10.1016/j.actamat.2014.04.022.
[29] C. Kirchlechner, Dislocation Slip Transfer Mechanisms : Quantitative Insights from in situ Micromechanical Testing, Habilitation Thesis, Montanuniversität Leoben, 2017.
[30] N.V. Malyar, H. Springer, J. Wichert, G. Dehm, C. Kirchlechner, Synthesis and mechanical testing of grain boundaries at the micro and sub-micro scale, Mater. Test. 61 (2019) 5–18, doi:10.3139/120.111286.
[31] C. Kirchlechner, J. Keckes, C. Motz, W. Grosinger, M.W. Kapp, J.S. Micha, O. Ulrich, G. Dehm, Impact of instrumental constraints and imperfections on the dislocation structure in micron-sized Cu compression pillars, Acta Mater 59 (2011) 5618–5626, doi:10.1016/j.actamat.2011.05.037.
[32] D. Kiener, C. Motz, G. Dehm, Micro-compression testing: A critical discussion of experimental constraints, Mater. Sci. Eng. A. 505 (2009) 79–87, doi:10.1016/j.msea.2009.01.005.
[33] R. Dou, B. Derby, A universal scaling law for the strength of metal micropillars and nanowires, Scr. Mater. 61 (2009) 524–527, doi:10.1016/j.scriptamat.2009.05.012.
[34] L.C. Lim, R. Raj, Continuity of slip screw and mixed crystal dislocations across bicrystals of Nickel at 573 K, Acta Metall (1985) 33, doi:10.1016/0001-6160(85)90057-4.
[35] L. Lu, X. Chen, X. Huang, K. Lu, Revealing the maximum strength in nanotwinned copper, Science 323 (2009) 607–610, doi:10.1126/science.1167641.
[36] P. Sudharshan Phani, K.E. Johanns, E.P. George, G.M. Pharr, A simple stochastic model for yielding in specimens with limited number of dislocations, Acta Mater 61 (2013) 2489–2499, doi:10.1016/j.actamat.2013.01.023.
[37] T.A. Parthasarathy, S.I. Rao, D.M. Dimiduk, M.D. Uchic, D.R. Trinkle, Contribution to size effect of yield strength from the stochastics of dislocation source lengths in finite samples, Scr. Mater. 56 (2007) 313–316, doi:10.1016/j.scriptamat.2006.09.016.